Publishing Excellence
Inspiring Progress

ISSN: 0000-0000 www.aristonpubs.com/journal/science-of-optics-and-photonics https://doi.org/10.69626/sop.2026.0029

RESEARCH ARTICLE

Unlocking the Potential of Tin – Based Perovskite Solar Cells through Hole Transport Layer Engineering

Shatrughan Mishra[1], Pooja Lohia[1*], D.K. Dwivedi[2], Akash Anand Verma[3]

ABSTRACT: Focusing on the next generation of lead-free photovoltaics, this study presents a comprehensive comparison of $CH_3NH_3SnI_3$-based tin perovskite solar cells (PSCs), emphasizing the influence of various hole-transporting layers (HTLs) on their performance and operational stability. A comparative assessment of organic and inorganic HTLs using SCAPS-1D simulations, focusing on their effects on performance and spectral response has been investigated. Notably, TAPC (1,1-Bis[(di-4-alkylamino)phenyl]cyclohexane) emerged as a superior HTL candidate, enabling an outstanding efficiency of 31.82% at bulk material thickness of 0.3 µm, with an open circuit voltage(Voc) = 1.19 V, Short circuit current density(J_{SC}) 32.20 mA/cm^2, fill factor(FF) 82.73 and delivering quantum efficiency about90% across the wavelength range 400–800 nm range due to the efficient optical absorption and minimal recombination losses, effectively capturing the full visible light spectrum. These results represent an important step forward for tin-based perovskite systems, as they show TAPC's possibility of establishing the performance gap between lead-based and eco-friendly solar cells.

Keywords: Perovskite; PTAA; TAPC; HTL; Spiro-OMeTAD.

Received: 15 May 2026; Revised: 29 July 2026; Accepted: 05 August 2026; Published Online: 29 August 2026

1. INTRODUCTION

Perovskite-based solar cells have become popular in the photovoltaic sector because of lower production costs and higher power conversion efficiency (PCE). Traditional PSCs uses lead (Pb)-based materials, which have contentious environmental issues and health risks because of lead toxicity. Therefore, there is great interest in materials that are environmentally benign and can develop into a useful perovskite solar cell. One alternative is tin-based perovskites with regard to the lead-based perovskite methylammonium tin iodide ($CH_3NH_3SnI_3$). Tin is an earth - abundant and non-toxic element, so it can better aid in PSCs sustainability. However, many inconsistencies still exist for tin-based perovskite to report highly efficient PSCs due to instability like oxidation and defects [1, 2]. The Sn^{2+} oxidation is a problem but due to some strategies like Antioxidant additives like cesium trifluoroacetate, 2D material integration and coordination chemistry (use of coordination nanosheets) are the different techniques by which the oxidation issue of tin(Sn) based perovskite can be minimized. The choice of HTL plays a significant role in the overall performance of perovskite solar cells. Depending on the efficiency of removing the +ve charges (holes) from the layer of perovskite to the electrode to charge makes a significant HTL impact on photovoltaic results. Further, varying organic and inorganic materials has been investigated as "HTL" to improve efficiency in perovskite photovoltaic cells [3]. The outcomes of this work will support to the development of high-efficiency, stable, and environment friendly

[1] Department of Electronics and Communication Engineering Madan Mohan Malaviya University of Technology, Gorakhpur-273010, U.P, India
[2] Photonics and Photovoltaic Research Lab (PPRL) Department of Physics and Material Science Madan Mohan Malaviya University of Technology, Gorakhpur- 273010, India
[3] Department of Physics Udit Narayan Post Graduate College, Padrauna, Kushinagar-274304, U.P, India

[*] Author to whom correspondence should be addressed: lohia.pooja6@gmail.com (P. Lohia)

© Ariston Publications 2026. All rights reserved.

PSCs, providing the way for the practical application in sustainable energy solutions.

To meet the growing global need for effective solar technologies that do not use toxic materials or threaten our environment, tin-based perovskites, i.e., $CH_3NH_3SnI_3$, offer a suitable choice to lead-based materials. This work is aimed on the profiling of $CH_3NH_3SnI_3$-based PSCs with a specific focus on how different HTL materials interact to improve solar cell performance. The design of the $CH_3NH_3SnI_3$ solar cells employed a consistent electron-transporting layer (ETL) with a variety of different HTLs, using SCAPS-1D simulations to compare PCE, spectral response, and high stability of solar cells [4, 5]. Results from the simulation confirmed that the HTL was an essential consideration when assessing the potential efficiency and operational reliability of the tin-based PSCs design. Within the materials available, organic HTL (TAPC, Spiro-OMeTAD and PTAA) are chosen, where TAPC stands for (1,1 Bis(di 4 tolylaminophenyl)cyclohexane) is a high mobility HTL widely used in PSCs and OLEDs (Organic Light emitting Diode) for efficient charge transfer. Spiro OMeTAD, a spirobifluorene derivative, is a benchmark HTL in PSCs and OLEDs, valued for stability and charge mobility. PTAA (Poly[bis(4 phenyl)(2,4,6 trimethylphenyl)amine]) is a polymeric HTL offering tunable energy levels and solution processability for perovskite devices. Inorganic $CuSbS_2$ (copper antimony sulfide) is an earth abundant, non toxic semiconductor absorber for thin film solar cells, combining suitable bandgap (∼1.5 eV) with eco friendly composition produced the biggest increases in performance in devices, respectively [6]. Each HTL carried its unique benefits. A consistent common ETL (C_{60}) is used with all device configurations with different HTLs. C_{60}, a fullerene molecule, serves as an efficient ETL in perovskite and organic solar cells. Its high electron affinity, mobility, and ability to passivate defects enable effective charge extraction and reduced recombination, improving device stability and efficiency [7].

These HTL materials were compared systematically, and for each configuration, a decision was made for the overall efficiency to try to determine the best HTL to support solar cells made with Sn-based materials. A lot of previous research work also conducted with such tin- based perovskite material like (Md Nahiduzzaman Nahid et.al, 2024) demonstrated for FTO/STO/$CH_3NH_3SnI_3$/SPIRO OMeTAD device configuration structure with a PCE of 23.57% [8], (D. Sharma et.al, 2023) uses TCO/C_{60}/ $CH_3NH_3SnI_3$/$CuSbS_2$optimized device structure with the PCE of 25% [9], (RazikaZair et.al, 2021) demonstrate for Au/$CH_3NH_3SnI_3$/TiO_2/ZnO optimized device structure with PCE of 20.08 % [10], (Manas Tripathi et.al, 2022) demonstrate with FTO/SnO_2/$CH_3NH_3SnI_3$/SPIRO OMeTAD optimized device structure with a PCE of 22.21 % [11], (Ajay Kumar et.al 2023) represents for IGZO/(PEA)0.2(FA)0.8SnI_3/Cu_2O/Audevice structure provides the optimized PCE of 26.45% [12], (Tanzir Ahamed et.al, 2022) also demonstrate for glass substrate/FTO/TiO_2/$CH_3NH_3SnI_3$/CuI optimized device structure provides the highest PCE of 21% [13] and (Ipsita Mohanty et.al 2025) show their work for the optimized device structure Au/SnS/$CH_3NH_3SnI_3$/TiO_2/ZnO:Al with a maximum PCE of 21.89% [14] such that all of these device structures uses Sn based PSC. In this study work, the defect density ranges between 1x1013 to 1x1018 for the different layers in the solar cell. The main objective for using tin-based perovskites is the potential for them to be a non-toxic alternative to lead-based [15]. In addition to environmental considerations, some of these potential materials showed good efficiency once worthy of addressing their synthetic methods to use low-cost and simple solution-processing techniques. In this observation Along with high levels of work addressed on stability and maintaining performance levels of tin-based devices to real-world levels of stressors, address them to key aspects for photovoltaic devices [16–18]. In this study out of 4 different HTLs, the maximum efficiency with device structure TCO/C_{60}/$CH_3NH_3SnI_3$/TAPC is 31.82 %, similarly with TCO/C_{60}/$CH_3NH_3SnI_3$/PTAA is 28.40%, TCO/C_{60}/$CH_3NH_3SnI_3$/SPIRO-OMeTAD is 29.50% and TCO/C_{60}/$CH_3NH_3SnI_3$/$CuSbS_2$ is 27.40% respectively.

2. SIMULATION METHODOLOGY

This study presents a fundamental knowledge base for developing high-efficiency (PCE), lead-free PSCs, possibly facilitating future progress in sustainable photovoltaic with intelligent choices of HTL materials [19]. In order to optimize the possible performances of these Sn-based PSCs, we sought to empirically and systematically study the influence of different types of (HTLs), both organic and inorganic, on the PCE through SCAPS-1D simulations [20].

In this work, Main purpose is to use the SCAPS-1D simulation software tool for the analysis & simulation of Tin (Sn)-based PSC. This simulation software is a practical numerical modelling-based tool which is made to help good understanding and provides the sense of the real work of the solar

 © Ariston Publications 2026. All rights reserved.

Table 1. Input parameters required for the simulation proposed for photovoltaic solar cells [21–23].

Parameters	TCO	ETL C_{60}	Perovskite $CH_3NH_3SnI_3$	HTL PTAA	HTL TAPC	HTL SPIRO	HTL $CuSbS_2$
Thickness (nm)	500	50	450	80	100	100	20
E_g (eV)	3.5	1.7	1.3	2.960	3.5	3	1.4
χ (eV)	4.4	4.2	4.17	2.3	2.1	2.45	3.85
ε (relative)	9.0	4.2	8.2	9.0	10	3	8.2
N_c (cm^{-3})	2.2×10^{19}	8.0×10^{19}	1.0×10^{18}	1.0×10^{21}	1.0×10^{19}	2.2×10^{18}	2.0×10^{18}
N_v (cm^{-3})	1.85×10^{19}	8.0×10^{19}	1.0×10^{18}	1.0×10^{21}	1.0×10^{19}	1.85×10^{19}	1.0×10^{19}
μ_e (cm^2/Vs)	2.0×10^{1}	8.0×10^{-2}	1.60	1.0	50	2.0×10^{-4}	50
μ_h (cm^2/Vs)	1.0×10^{1}	3.5×10^{-3}	1.60	40	50	2.0×10^{-4}	50
N_D (cm^{-3})	2.0×10^{19}	2.6×10^{18}	1.0×10^{15}	0	0	0	0
N_A (cm^{-3})	0	0	1.0×10^{15}	2.0×10^{18}	1.0×10^{15}	1.5×10^{17}	1.38×10^{19}
N_t (cm^{-3})	1.0×10^{15}	1.0×10^{14}	1.0×10^{13}	2.0×10^{14}	1.0×10^{14}	1.0×10^{15}	1.0×10^{14}

system. There are various simulators too like GVPDM and Silvaco, but they are complicated and require extra time for the processing [24][21]. All SCAPS-1D simulation results (except the result of Temp. variation) are used the light intensity of the Airmass(AM-1.5) light spectrum at 300 K. The densities of Charge Carriers (e- and holes) have been determined by using the continuity and Poisson equations shown in the given expression [25, 26].

$$\frac{d}{dx}\left(\varepsilon(x)\frac{d\psi(x)}{dx}\right) = q\left[N_D^+(x) - n_t(x) + p_t(x) + n(x)p(x) - N_A^-(x)\right] \quad (1)$$

$$\frac{\partial p}{\partial t} = \frac{1}{q}\nabla \cdot J_p - R_p + G_p \quad (2)$$

$$\frac{\partial n}{\partial t} = \frac{1}{q}\nabla \cdot J_n - R_n + G_n \quad (3)$$

In the above equations:

ϕ, q represents the potential and charge, $n(x)$, $n_t(x)$, G_n, R_n & J_n represents the concentration, Trap concentration, generation rate, recombination rate and e-current density. Similarly $p(x)$, $p_t(x)$, R_p, G_p and J_p again represents as concentration, trap concentration, recombination rate, generation rate and current density of hole. ϵ signifies the dielectric permittivity of material, while $N_D^+(x)$ and $N_A^-(x)$ gives the donor and acceptor density [27].

Each HTL was simulated with its own unique set of input parameters, reflecting its material-specific properties Table 1 & 2. The selection of proper band gap (E_g) is also essential by using 2.96 eV, 3.5 eV, 3 eV and 1.4 eV for PTAA, TAPC, SPIRO and $CuSbS_2$ HTLs respectively. The primary objective was to compare the simulation outcomes and identify the HTL that delivers the highest PCE when paired with $CH_3NH_3SnI_3$ under standard illumination conditions [28].

Table 2. Types of interface defect parameters.

Parameters	HTL/Bulk layer	Bulk layer/ETL	ETL/TCO
Defect type	Neutral	Neutral	Neutral
Capture cross section of e^- (cm^2)	1.00×10^{-19}	1.00×10^{-19}	1.00×10^{-19}
Capture cross section of holes (cm^2)	1.00×10^{-19}	1.00×10^{-19}	1.00×10^{-19}
Energy distribution	Single	Single	Single
Energy level w.r.t. references (eV)	0.600	0.600	0.600
Interface defect density (cm^{-2})	1.00×10^{10}	1.00×10^{10}	1.00×10^{10}

Table 3. Comparison of the efficiencies of the designed cell with previously published research results.

Sr. No.	Device Configuration	Efficiency (%)	References
1	TCO/C_{60}/$CH_3NH_3SnI_3$/PTAA	28.40	[This study]
2	TCO/C_{60}/$CH_3NH_3SnI_3$/SPIRO OMeTAD	29.50	[This study]
3	TCO/C_{60}/$CH_3NH_3SnI_3$/$CuSbS_2$	27.20	[This study]
4	**TCO/C_{60}/$CH_3NH_3SnI_3$/TAPC**	**31.82**	**[This study]**
5	FTO/STO/$CH_3NH_3SnI_3$/SPIRO OMeTAD	23.57	[8]
6	TCO/C_{60}/$CH_3NH_3SnI_3$/$CuSbS_2$	25.0	[9]
7	Au/$CH_3NH_3SnI_3$/TiO_2/ZnO	20.08	[10]
8	FTO/SnO_2/$CH_3NH_3SnI_3$/SPIRO OMeTAD	22.21	[11]
9	IGZO/$(PEA)_{0.2}(FA)_{0.8}SnI_3$/$Cu_2O$/Au	26.45	[12]
10	Glass substrate/FTO/TiO_2/$CH_3NH_3SnI_3$/CuI	21	[13]
11	Au/SnS/$CH_3NH_3SnI_3$/TiO_2/ZnO:Al	21.89	[14]

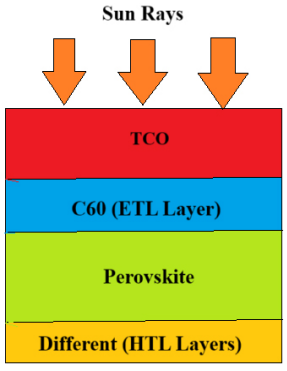


Fig. 1. Device structure of desired tin based Perovskite solar cell.

© Ariston Publications 2026. All rights reserved.

Figure 1 represents the device architecture of the proposed tin-based PSC. In this device configuration, the ETL is made-up of C_{60}, and the transparent conductive oxide (TCO) based layer remains consistent across all simulations [29]. The perovskite absorber (Bulk) layer employed is $CH_3NH_3SnI_3$ (methylammonium tin iodide), chosen for its favorable optoelectronic properties and reduced toxicity compared to lead-based counterparts. To assess the influence of HTLs on device performance, Four distinct materials were incorporated: three organic HTLs—TAPC, Spiro-OMeTAD, and PTAA and one inorganic HTL, $CuSbS_2$. Each HTL was integrated individually while keeping the other layers constant, enabling a systematic evaluation of their effect on the PCE of the solar cell [30, 31].

3. RESULTS AND DISCUSSIONS

3.1 Effect of Perovskite layer thickness on performance

Figure 2a - 2d represents the influence of perovskite layer thickness on key photovoltaic performance metrics for four different hole transport layers (HTLs): TAPC, SPIRO, PTAA, and $CuSbS_2$ respectively.

Figure 2a provides the insightful knowledge that PCE generally increases with perovskite thickness for all HTLs, it peaks around 0.8–1.0 µm. TAPC consistently gives the highest efficiency across all different thickness level; it indicates the superior charge extraction and minimal recombination losses. SPIRO follows closely, while PTAA and $CuSbS_2$ are lagging behind, suggesting less effective hole transport or higher interfacial recombination. Figure 2b presents the Voc trends, TAPC and SPIRO maintain relatively stable and high Voc values across the thickness range, which shows the good energy level alignment and low recombination. Where, PTAA and $CuSbS_2$ provides a decline in Voc with increasing thickness, which shows due to enhanced bulk recombination or poor interface quality at higher thicknesses [32]. Figure 2c shows J_{SC} behavior. TAPC and SPIRO are representing a steady increase in J_{sc} with thickness, which attributed to improved light absorption and efficient carrier collection. $CuSbS_2$ curve, despite starting with low J_{sc}, it shows a sharp rise at higher thicknesses, possibly due to enhanced absorption but itsuffer from poor charge extraction. PTAA's J_{sc} increases modestly, indicating moderate performance. Figure 2d reveals Fill Factor trends, As TAPC and SPIRO shows high FF values, suggesting low series resistance and efficient charge transport. PTAA and $CuSbS_2$ reflect the decreasing FF with thickness, implying increased resistive losses or poor interface contact.Asa overall results discussions, we are concluded that TAPC emerges as the most promising HTL across all thicknesses because it offers the balanced performance in all parameters. SPIRO also performs well, while PTAA and $CuSbS_2$ show limitations, especially at higher thicknesses. This comparative analysis helps a lot in selecting optimal HTLs for the designing of efficient perovskite solar cell.

3.2 Variation of key Parameters with change in Defect Density (N_t)-

Figure 3a - 3d demonstrates how the N_t affects the main performance parameters of photovoltaic of PSCs using various HTLs: TAPC, SPIRO, PTAA, and $CuSbS_2$. These plots provide the data on the impact of intrinsic and interfacial defects on the performance of the devices with different sets of HTL. Figure 3a demonstrates an inverse relationship that is evident between PCE and Nt. The PCE decreases with the defect density between 1013 and 1018 cm^{-3} which is the range of defect density of all HTLs. The PCE of TAPC is the highest amongst the entire N_t range, followed by Spiro, PTAA and $CuSbS_2$. This tendency justify the fact that TAPC has better defect tolerance, which is probably caused by less recombination at the interface and better energy level chosen. Figure 3b indicates Voc degradation at a higher Nt. The non-radioactive recombination is more evident as Voc dropdown decreases sharply at 1013 and 1018 cm^{-3} of all HTLs. TAPC and Spiro have higher Voc values and this indicates that they inhibit the defect-assisted process of recombination. $CuSbS_2$ is the one with the greatest degradation, which indicates the reduced interface passivation and increased trap-assisted recombination. Figure 3c is a plot of J_{sc} and varying values of HTLs where J_{sc} declines with increasing as N_t with TAPC and Spiro exhibit sluggish degradation as compared to the others. This means that such materials make the collection of carriers easier in cases where there are defects. $CuSbS_2$& PTAA has lower J_{sc} at beginning and worse degradation with time, it means that charge transport is weak and recombination losses are large. Figure 3d shows FF trends. FF reduces with rise in N_t which is in line with rising series resistance and recombination losses. TAPC and Spiro have the same high Fill factor values, and PTAA and $CuSbS_2$ have large values reduced, particularly at N_t above 1015 cm^{-3}. This shows that the charge transport pathways of TAPC and Spiro are more stable and the interface quality is high in comparison to PTAA

 © Ariston Publications 2026. All rights reserved.

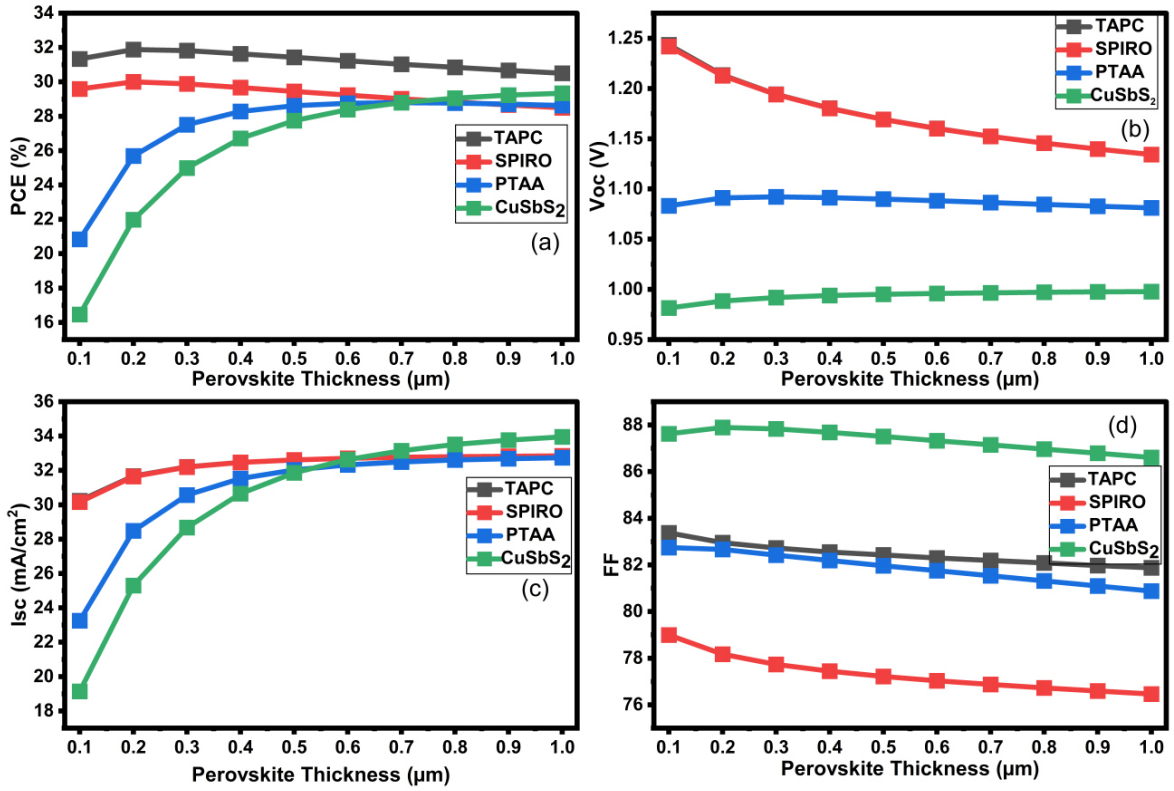


Fig. 2. Represents the graph between Key performance parameters (PCE, Voc, J_{SC}, FF) and change in thickness of different HTLs.

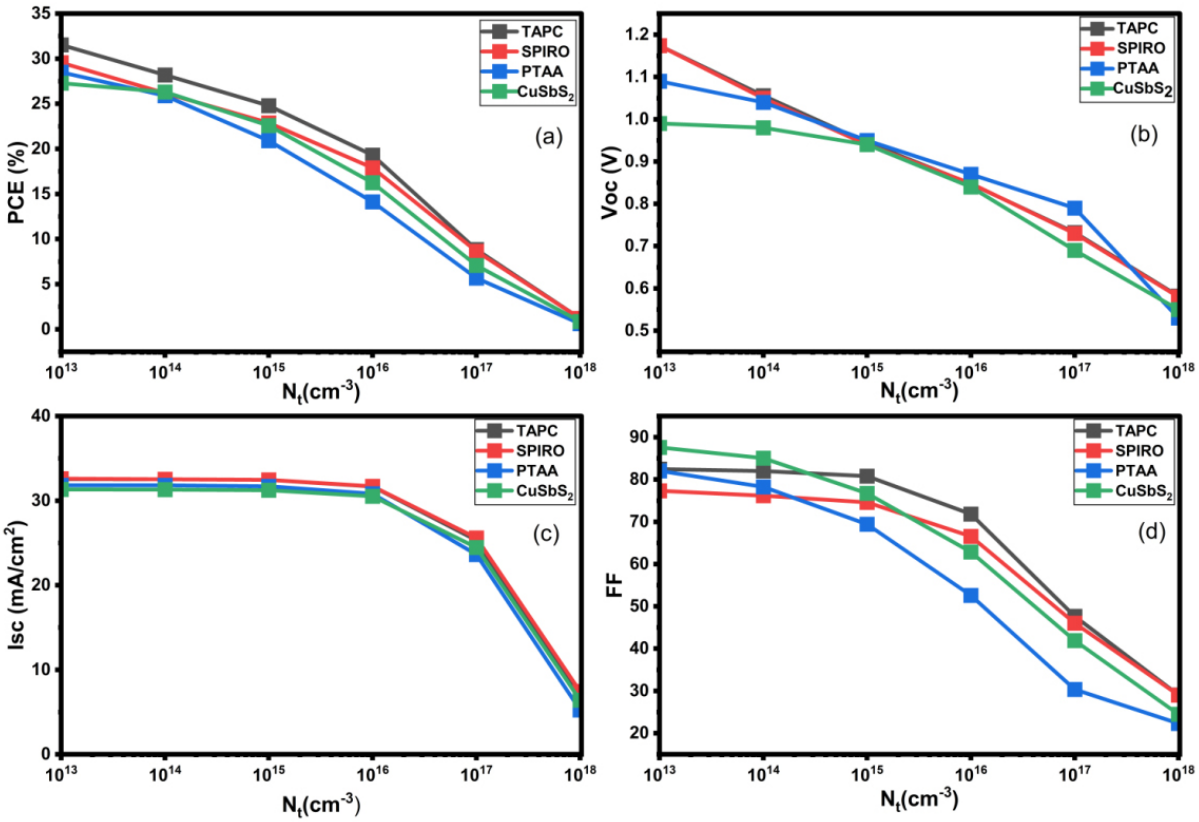


Fig. 3. Represents thevariation of key solar parameters as a function of Defect density (N_t) for various HTLs.

© Ariston Publications 2026. All rights reserved.

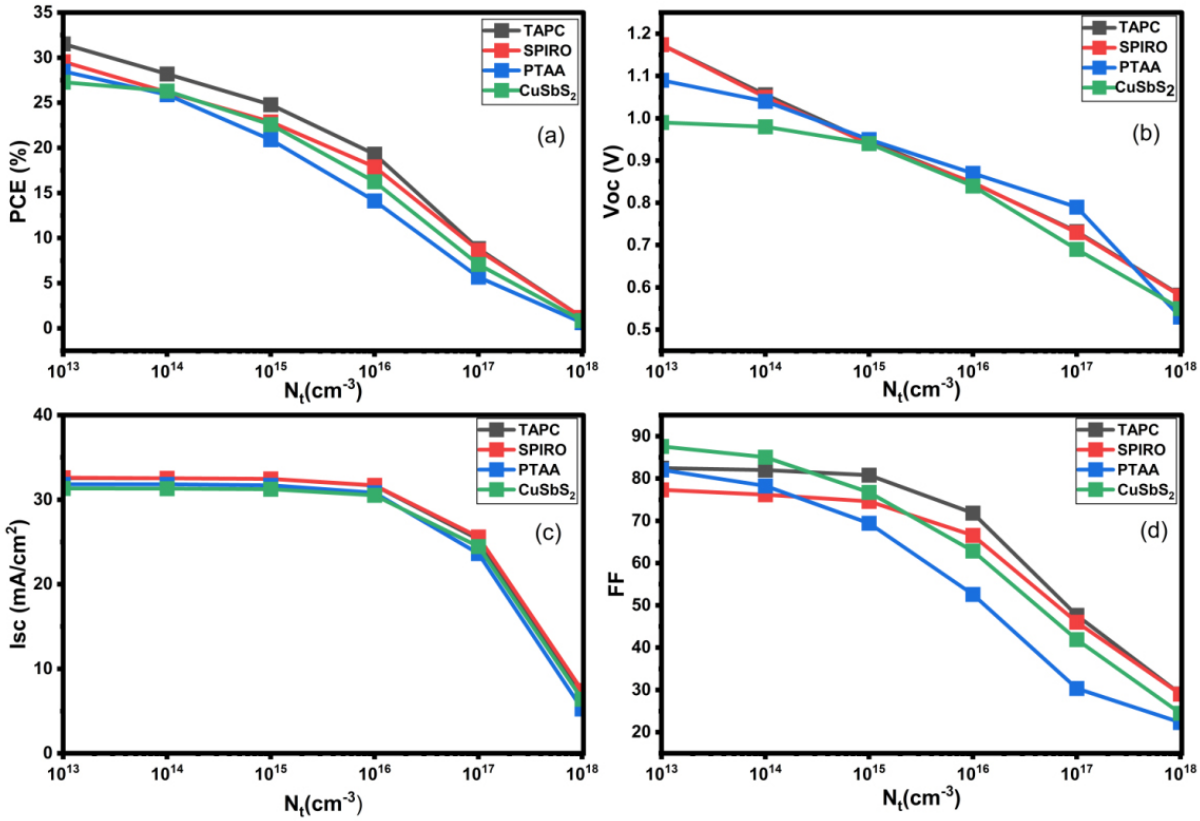


Fig. 4. Represents the effect of varying temperature on key performance Indicators (PCE,Voc,J_{SC} and FF)—

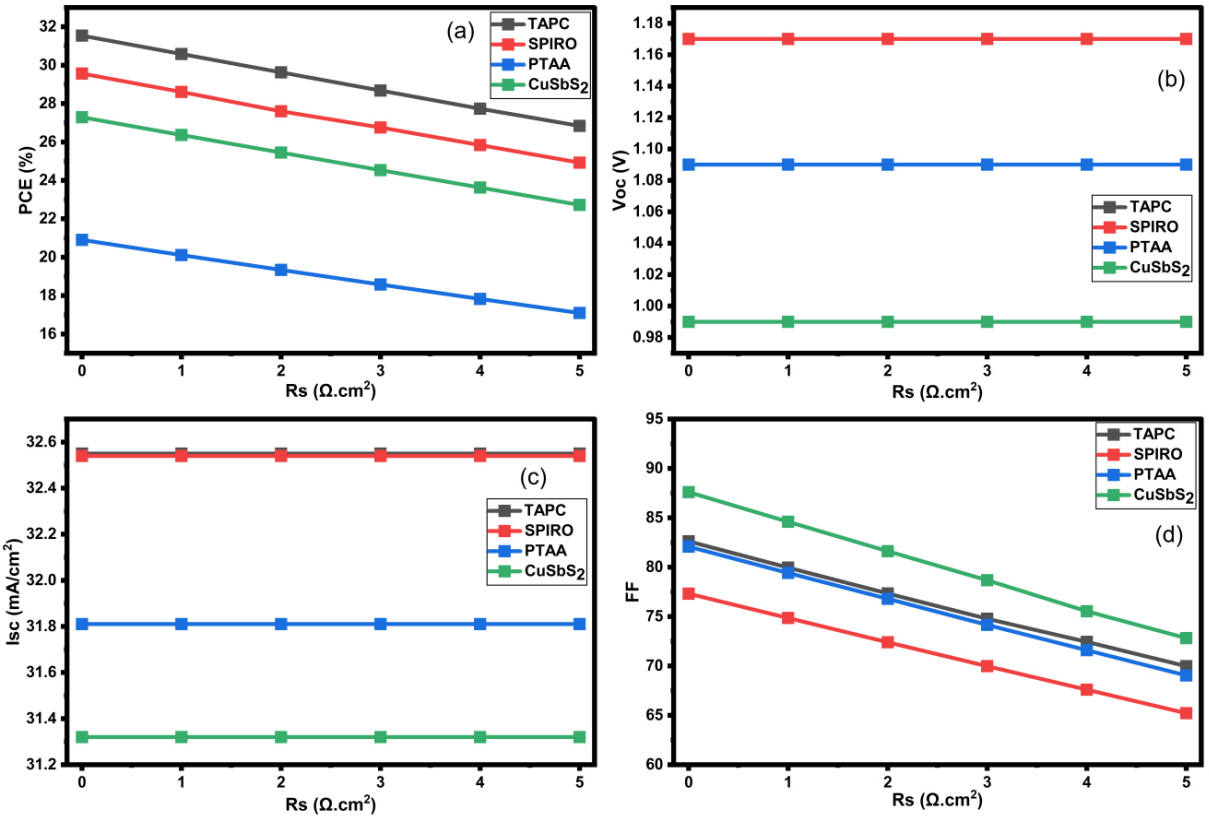


Fig. 5. Shows the influence of series resistance (Rs) on four critical photovoltaic performance parameters for the perovskite solar cells using different hole transport layers (HTLs): TAPC, Spiro, PTAA, and $CuSbS_2$.

 © Ariston Publications 2026. All rights reserved.

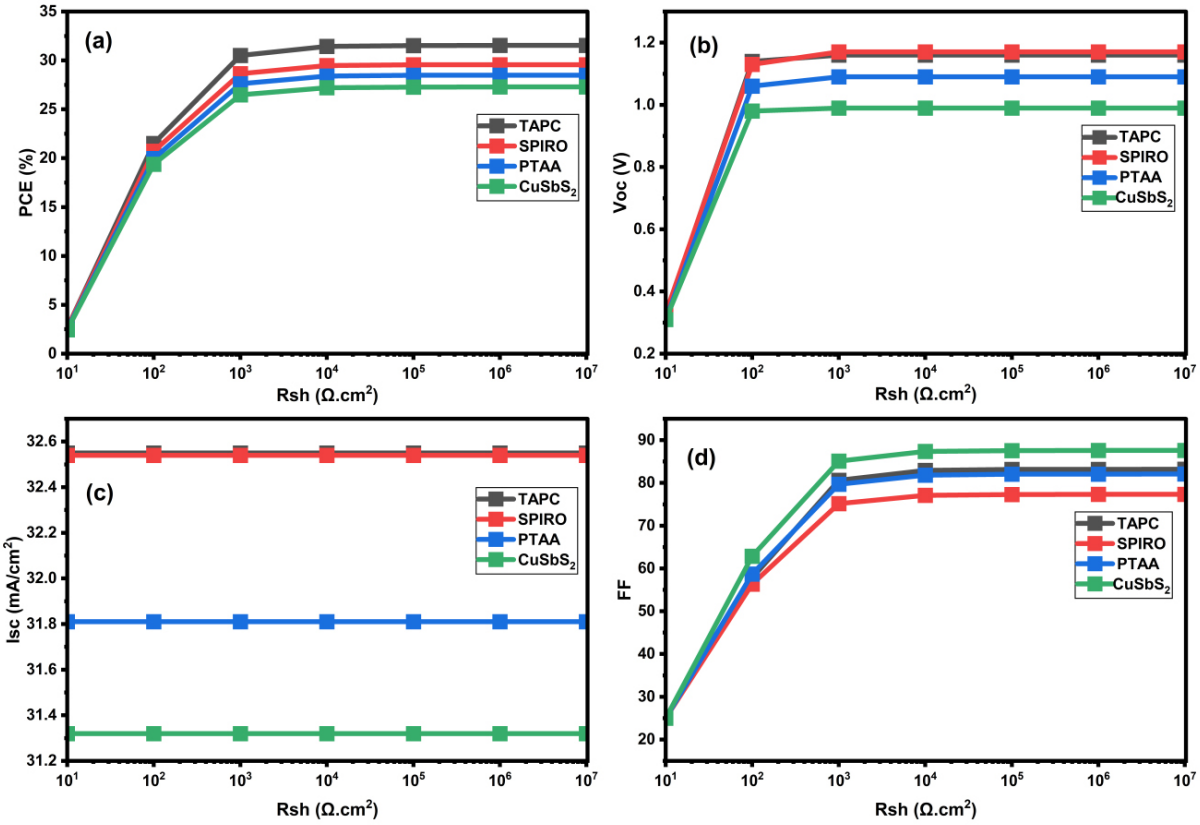


Fig. 6. Gives information of the effect of shunt resistance (R_{sh}) on four basic photovoltaic parameters. For the perovskite solar cells using different above mentioned HTLs. The x-axis represents the logarithmic value range of R_{sh} from 101 to 107 Ω·cm^2 and it describe how the leakage pathways are influencing the device performance.

and $CuSbS_2$. Simply put, TAPC has always been superior to other HTLs at all defect densities due to its good resistance to defect-related degradation. Spiro also demonstrates the acceptable performance, whereas PTAA and $CuSbS_2$ is more sensitive to defect density, and therefore it is only applicable to defect-prone environments. This finding indicates that it is necessary to choose HTLs with high defect tolerance to achieve stable and efficient perovskite solar cell functioning.

3.3 Effect of Temperature on key performance parameters-

Figure 4a - 4d shows the temperature-dependent behaviour of the perovskite solar cells with the various HTLs: TAPC, Spiro, PTAA, and $CuSbS_2$ added. The graphs can give information on thermal stability and performance degradation mechanisms of HTL choices. Figure 4a reveals that all HTLs have a negative correlation between temperature and PCE. TAPC is the most efficient at all temperatures, and it is then closely followed by Spiro, PTAA, and $CuSbS_2$. It is believed that the deterioration of PCE is due to the increased non-radiative recombination and the decreased carrier mobility under high temperatures. The high thermal stability of TAPC indicates high-quality interface and low level of energy levels discrepancy during thermal stress.

Figure 4b illustrates the degradation of Voc with increasing temperature. For all HTLs, Vocdecreases approximately linearly, a trend consistent with the thermodynamic relation,

$$V_{oc} \propto \ln(J_{sc}) - \ln(J_0) \tag{4}$$

Where J_0 (the reverse saturation current density) increases with temperature due to enhanced recombination [33, 34]. TAPC and Spiro have a higher Voc value, which means that they have better suppression of thermally activated recombination. $CuSbS_2$ exhibits the strongest decrease, indicating the inability to passivate defects as well as trap-assisted recombination that is more active at higher temperature. Figure 4c depicts that J_{sc} is temperature-dependent, showing that the higher the temperature, the stronger the recombination process is. This is because the carrier generation is increased and the bandgap is reduced at high temperatures which increases light absorption. Interestingly, $CuSbS_2$ has the highest J_{sc} which is probably

© Ariston Publications 2026. All rights reserved.

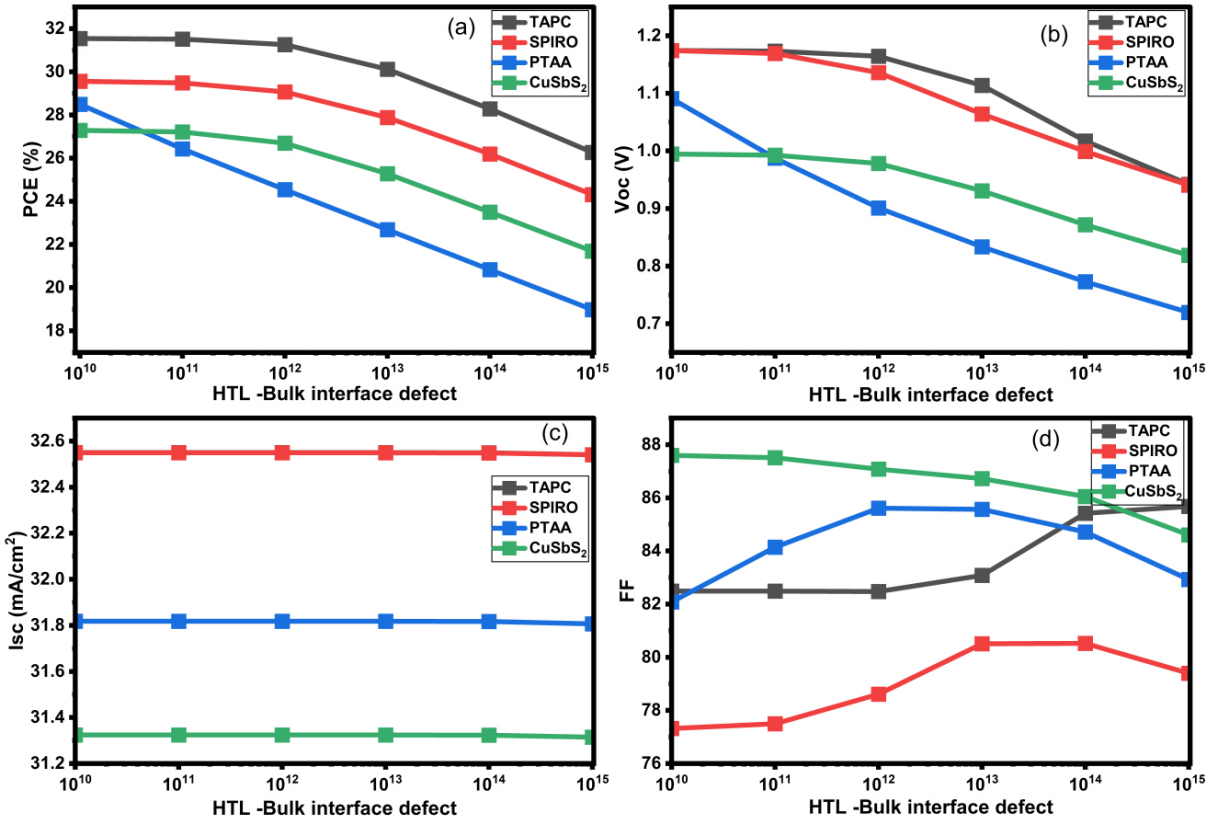


Fig. 7. Represents the variation of HTL –Bulk interface Defect Density(N_t) with all four key parameters(PCE, Voc, Isc, FF)

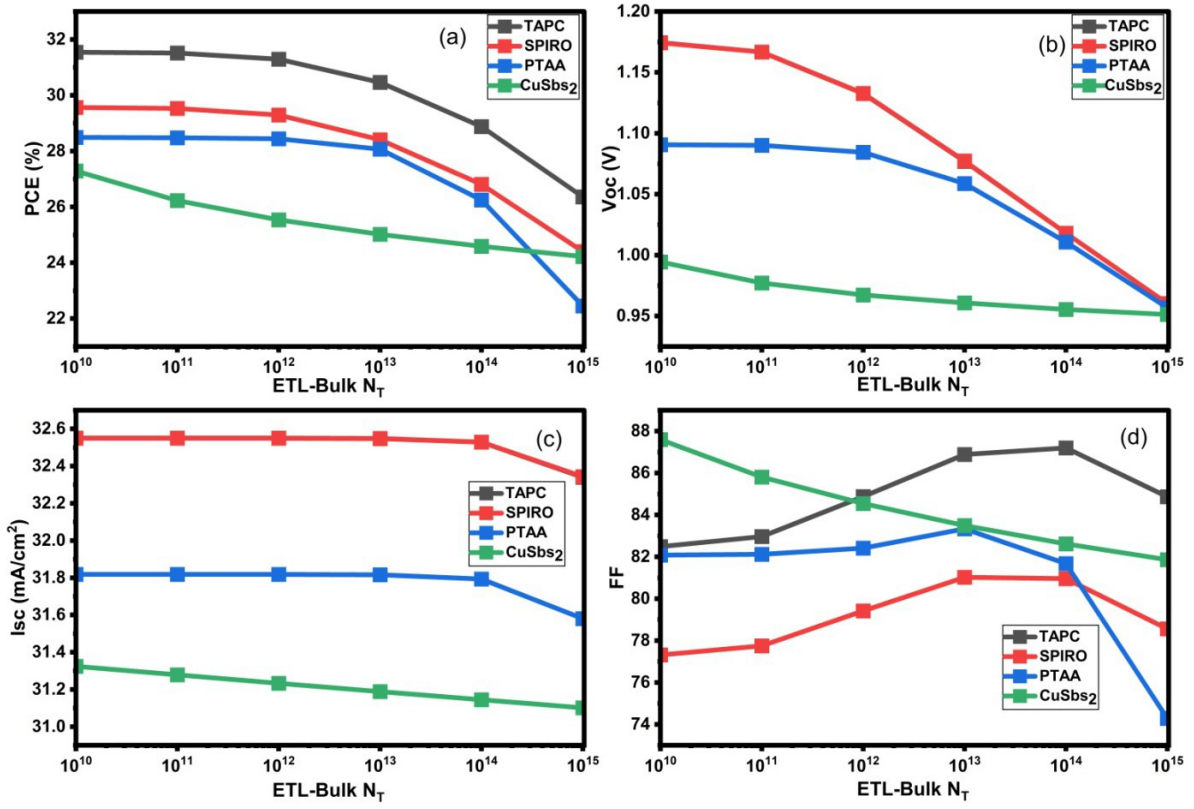


Fig. 8. Represents the variation ETL-Bulk interface Defect Density (N_t) with all four key parameters(PCE, Voc, Isc, FF)

 © Ariston Publications 2026. All rights reserved.

because it has wider absorption spectrum and good band positions to generate charges. Nonetheless, its total results are not very successful because of the low Voc and FF. Figure 4d indicates that FF declined as temperature rise. The cause of this decrease is attributed to the augmented series resistance and decreased carrier mobility, which deteriorate the extraction of charges. TAPC and Spiro have larger values of FF implying that they have strong charge transport and low resist losses. There is a high FF degradation in PTAA and $CuSbS_2$ suggesting that it is less thermally robust. On the whole, TAPC is the most thermally stable HTL, which retains high PCE, Voc, and FF throughout the temperature range. There is also good performance by Spiro, PTAA and $CuSbS_2$ are more susceptible to thermal degradation. These results demonstrate the necessity to choose HTLs with high thermal stability to obtain effective perovskite solar cells functioning under different environmental conditions.

3.4 Effect of Series Resistance (R_s)

Figure 5a indicates that there is an inverse relationship between PCE and R_s With the rise in Rs, PCE goes down (it is inversely related to both) in all forms of HTLs because the amount of resistive loss increases and opposes the extraction of the charge and the total device efficiency decreases. It is demonstrated that TAPC always has the highest PCE in the entire range of Rs, with Spiro, PTAA, and $CuSbS_2$ coming next, which implies that this device has the best charge transport and the least degradation due to resistance. The reflection of Figure 5b is that Voc is not very sensitive to variations in series resistance (Rs). This should be because Voc is mostly dictated by the quasi-Fermi level splitting and recombination dynamics which do not necessarily depend on the series resistance directly. TAPC has the highest Voc, indicating improved quality of the interface and low values of recombination and $CuSbS_2$ has the lowest values. As illustrated in Figure 5c, it is also clear that J_{sc} is independent of all HTLs as well as independent of varying R_s This means that series resistance does not play a major role on photogenerated current in ideal conditions of illumination. Nevertheless, TAPC and Spiro have higher J_{sc} values indicating an improved carrier mobility and efficiency of collection. The sensitivity of FF to R_s is made evident in Figure 5d. FF reduces drastically with rising R_s since improved voltage drops in the IV curve. TAPC and Spiro have a higher value of FF, which implies a good ability to transport charges and low internal resistance. The FF degradation of PTAA and $CuSbS_2$ is more severe, which reduces their workability. Finally, Voc and J_{sc} are not affected, but PCE and FF are very sensitive to series resistance. TAPC is the strongest HTL as good alternative in high-efficiency and low-loss perovskite solar cells.

3.5 Effect of Shunt Resistance (R_{sh})

Figure 6a indicates that PCE outperforms the growth in R_{sh} of all HTLs. At the low Rsh, the leakage currents prevail and this lowers the effective output power. These losses reduce as we raise the Rsh, therefore enabling the intrinsic performance of the HTLs to come up. TAPC and Spiro has always exhibited the greater values of PCE in the range of R_{sh} that is selected which points to the greater suppression(reduction) of the leakage currents and the improved quality of the interface. PTAA and $CuSbS_2$ place emphasis on the reduced PCE particularly since at low R_{sh} indicates the increased vulnerability to the parasitic shunting. Figure 6b shows Voc variations against various HTLs. Voc rises with R_{sh} and levels off in the high ranges as shunt pathways are reduced to a minimum. TAPC and Spiro once more exhibit increased Voc at each value of R_{sh}, indicating the efficient energy level match and less recombination. $CuSbS_2$ has the smallest Voc, as it has poor interface passivation and defect-based recombination process. Figure 6c indicates that J_{sc} does not change significantly within the R_{sh} range of all the HTLs since photogenerated current is not very sensitive to shunt resistance under normal illumination condition, provided that leakage is not dominant. TAPC and Spiro once more give rise to the J_{sc} which implies an efficient collection of carriers and low recombination losses. Figure 6d indicates that the value of FFis directly proportional to the Rsh. Low R_{sh} FF results at low values because of leakage currents that deviate the I-V curve. The FF also improves with a rise in R_{sh} which exhibits the superior diode performance and reduced parasitic losses. The FF values of TAPC and Spiro are higher when compared to the values of PTAA and $CuSbS_2$ two at lower R_{sh} because of the existence of greater inside losses. As an Overall summarized finding, high shunt resistance enhances the performance of solar cell due to reduction in leakage and enhancement of the diode nature. TAPC and Spiro exhibit the highest performance in shunting effects thus proving them as the best HTLs in stable and efficient perovskite solar cells.

3.6 Effect of HTL-Absorber layer interfacial defect density

Figure 7a - 7d reflects the effect of HTL–Bulk

© Ariston Publications 2026. All rights reserved.

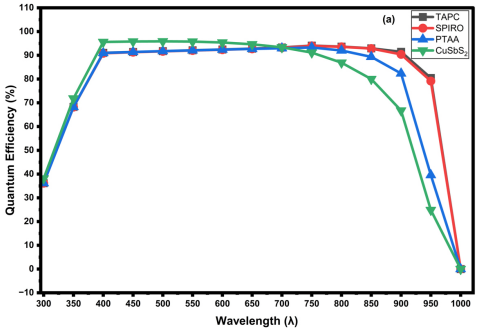


Fig. 9. Represents the Wavelength Vs Quantum efficiency.

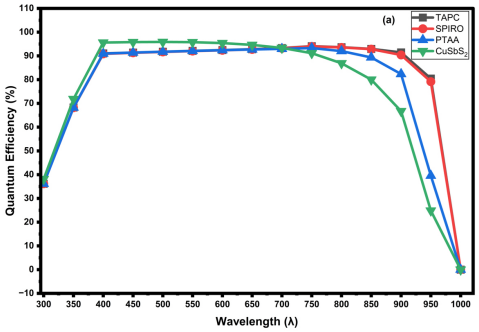


Fig. 10. Reflects the J-V curve with different HTLs.

interface defect density (N_t) on the basic photovoltaic parametersfor PSCs using variousabove mentioned HTLs. The defect density ranges lies between 1010 to 1015 cm^{-3}, capturing the behavior due to interfacial recombination. Figure 7a reveals that all HTLs have a sharp decrease in PCE with Nt. TAPC has the best efficiency in the entire defect range then Spiro, PTAA, and $CuSbS_2$are in descending order. Enhanced non-radiative recombination at the HTL- bulk material interface is the main cause of decay in PCE that decreases carrier lifetime and extraction efficiency. Figure 7b is Voc graph that also exhibits the same trend as in PCE. Voc decreases a lot with Nt, indicating the augmented recombination losses which decrease the quasi-Fermi level splitting. The higher Voc value is found in TAPC and Spiro that implies the superior interface passivation and alignment of energy levels. $CuSbS_2$ exhibits the highest rate of decay, hence, the inferior quality of the interfaces and the high densities of the traps. Figure 7c shows J_{sc} behaviour, As J_{sc} is less sensitive to N_t than Voc and PCE, it tends to decrease with the increase in defect density very slowly. The values of J_{sc} are larger in TAPC and Spiro than in PTAA and $CuSbS_2$, which means that efficient carrier collection occurs despite increasing recombination. Figure 7d highlights FF graph, FF depends on N_t inversely because interface defects cause resistive losses and distort the I-V curve. TAPC and Spiro have a higher FF, whereas PTAA and $CuSbS_2$ reach more critical drops, which is limiting to its practical use. TAPC is also more tolerant to interface defects in Overall result anaylsis with higher PCE, Voc, J_{SC}, and FF over the wide N_t range. It demonstrates its appropriateness in the stable and efficient environment of PSCs, particularly in the defect prone fabrication conditions.

3.7 Effect of ETL-Absorber layer interfacial defect density-

Figure 8a - 8d shows the effect of ETL–bulk interface defect density (N_t) on four basic photovoltaic parameters for perovskite solar cells using different HTLs such as TAPC, Spiro, PTAA, and $CuSbS_2$ while a single ETL as C60. The defect density lies between 1010 to 1015 cm^{-3}, here we are checking the degree of degradation behavior due to the trap-assisted recombination on increasing the ETL- Bulk defect density. Figure 8a indicates that PCE is on the decline as N_t increases in all HTLs. There is also a similar case of TAPC with the highest efficiency in the entire range of defects, followed by Spiro, PTAA, and $CuSbS_2$. This reduction in PCE is as a result of non-radiative recombination at the ETL interface reducing carrier lifetime and extraction efficiency. Figure 8b presents Voctrends,Voc decreases with N_t and this indicates the effect of recombination on the quasi-Fermi level splitting. TAPC and Spiro maintain a larger value of Voc with PTAA and $CuSbS_2$ having the lower value implying superior interface passivation and energy level alignment. Figure 8c shows J_{SC}behavior. Though J_{sc} is not as sensitive to N_t as that of Voc and PCE, it decreases slightly as the defect density increases. The values of J_{sc} of TAPC and Spiro are larger than those of PTAA and $CuSbS_2$, which demonstrates effective carrier generation and collection owing to the higher rate of recombination and lower charge transport. Figure 8d points out to FF degradation, FF declines with rise in Nt, interface defects add resistive loss, distort the I-V curve. Increasing values of FF with case of TAPC and Spiro, whereas PTAA and $CuSbS_2$are significantly decreased because the limiting their working capabilities. The overall results, TAPC as HTL provides the highest ability to obtain tolerances to ETL-bulk interface defects, therefore preserving high PCE, Voc, J_{SC}, and FF throughout the N_t range.

3.8 Effect of Wavelength Vs Quantum efficiency-

The graph above depicts the quantum efficiency (%) & wavelength (nm) of PSCs using various HTLs that are expressed in the graph Figure 9. The range

 © Ariston Publications 2026. All rights reserved.

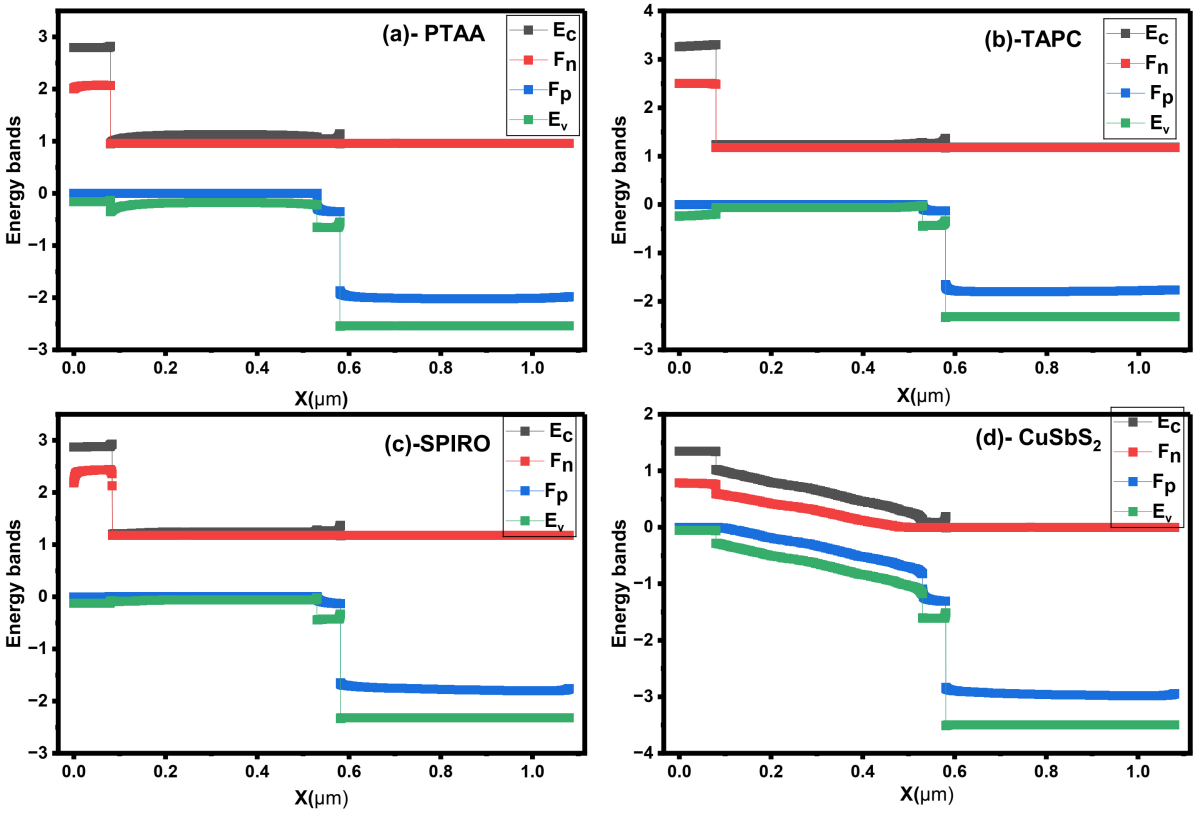


Fig. 11. Reflects the Energy band diagram with different HTL.

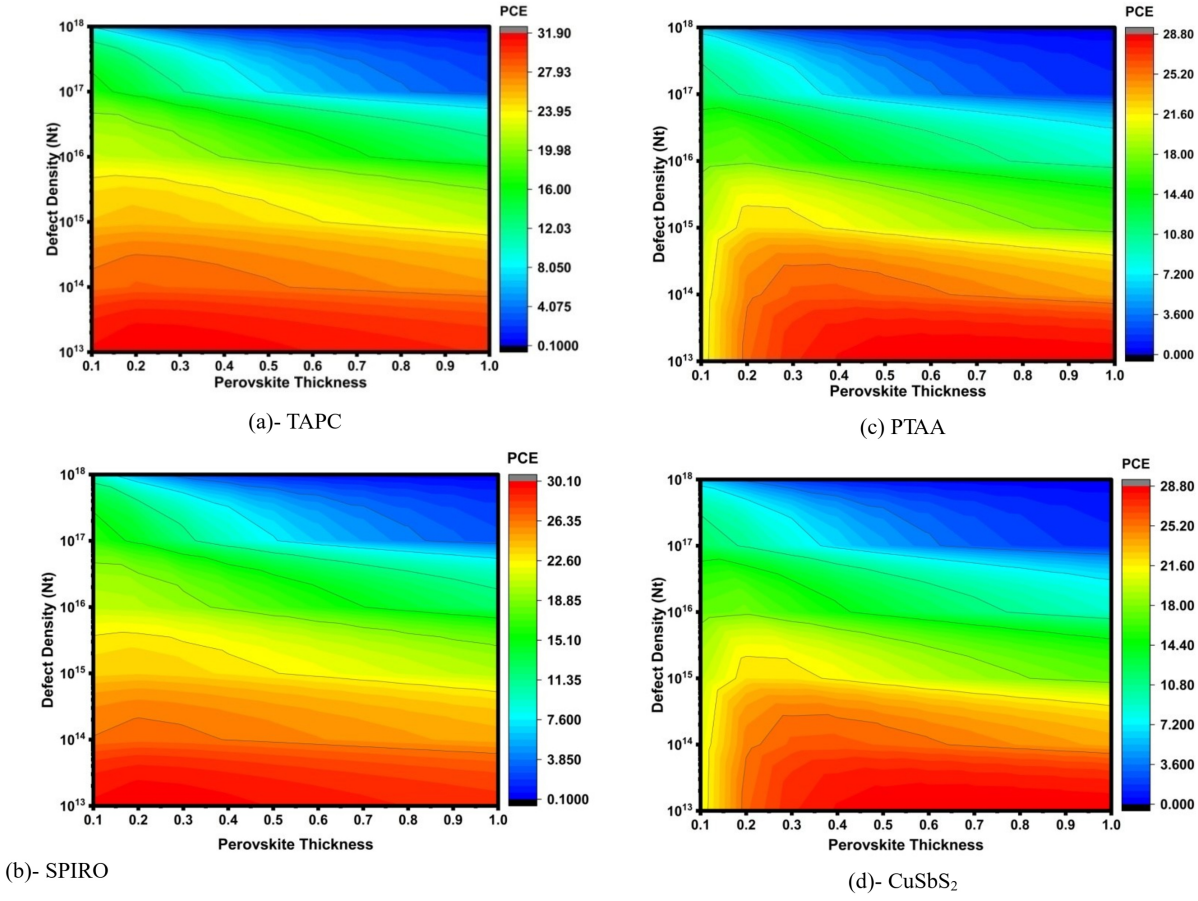


Fig. 12. Represents the contour plot with different HTL materials.

© Ariston Publications 2026. All rights reserved.

of wavelength lies between 300 nm and 1000 nm which includes the whole visible and near infrared spectrum that are of relevance to the solar energy harvesting process. All the HTL have high quantum efficiency in the central wavelength range (400-900 nm), This implies that they can absorb photons and generate carriers. TAPC and Spiro also exhibit high quantum efficiency, also, in the same way, they have almost 90% efficiency in a large part of the spectrum. This translates to the high charge extraction and low recombination losses hence they are very favorable in high-performance PSCs. PTAA and $CuSbS_2$ exhibit slightly limited quantum efficiencies especially at the higher wavelengths (above 800 nm). This can be as a result of poor alignment of the energy levels or enhanced recombination at the interface, which reduces the efficiency of the carriers in the near-infrared for carrier collection. TAPC is leading in all the ranges that underline its excellence in optical and electronic characteristics.

3.9 Represents the effect of J-V curve-

This Figure 10 demonstrates the graph between current density & voltage (J-V) curves of PSCs with the various HTLs: TAPC, Spiro, PTAA and $CuSbS_2$. The graph shows Jtot in (mA/cm^2) versus Voc, in (Volts). It provides the understanding of the electrical performance and charge transport characteristics of each HTL. The J-V profile of TAPC is the most desirable with a sharp increase in the current density, and high Voc, this signifies an effective charge extraction and minimum recombination losses. Spiro is a close follower of TAPC exhibiting the same behavior with a slightly smaller current output. $CuSbS_2$ exhibits the lowest values of Jtot and Voc, indicating lower quality of interfaces and increased recombination rates. $CuSbS_2$ on its part demonstrates almost a flat response up to approximately 1.0 V before the current density rises at an extremely rapid rate. As an Overall conclusion, the J-V curve affirm that TAPC and Spiro can provide better diode behavior and efficient photovoltaic work, whereas PTAA and $CuSbS_2$ experience resistive losses and recombination as it is represented in the graph. These trends are in line with previous performance measures, which is the significance of HTL choice in enhancing the efficiency of PSCs.

3.10 Represents the Energy band diagrams-

The above graph in the Figure 11a - 11d, reflects the energy band diagram with four different types of HTL.In each of the energy band diagram there are 4 curves in each figure, which are Ec, EV, Fnand Fp. These four curves in a graph are Conduction band, valance band and Fermi level for holes and electrons. In these graphs X-axis represents the variation on perovskite thickness and Y-axis provide us the information of energy band among all Ec, EV, Fnand Fp.

3.11 Represents the Contour plot to check the performance by varying the Perovskite thickness and Defect density -

This Figure 12 depicts four contour plots (a-d) that shows PCE in PSCs as a function of increasing perovskite layer thickness as well as the defect density, based on the selection of HTL. The subplots are associated with the various HTL as indicated in the graph. The x-axis of both subplots looks at the thickness of perovskites, and the y-axis is used to look at the defect density (N_t) in cm^{-3}. The gradient of colours, namely blue to red, shows the rising performance in terms of PCE with the red areas indicating the highly optimal performance areas. The plots play a vital role in knowing the material selection and fabrication parameters that affect the solar cell efficiency. Here, it can be clearly seen that TAPC exhibits high PCE in a small range of low defect density and moderate thickness which is indicative of sensitivity to defects. Spiro is more tolerant, retains high PCE in a larger thicknesses and defect density range, is robust though it might become more costly. PTAA exhibits a similar style as Spiro although slightly lower peak efficiency, it suggests good performance but perhaps less tolerance to defects compared to TAPC and Spiro. Although the inorganic HTL $CuSbS_2$ is a less common inorganic material, exhibits least overall PCE due to its ability to imply reduced compatibility or increased losses through recombination. These plots bring out the comparison of the organic and inorganic HTLs and their efficiency. Organic HTLs such as TAPC are more effective and defect-tolerant, whereas inorganic materials such as $CuSbS_2$ can be more stable and less efficient. In the process of determining the most appropriate fabrication windows, low densities of defects and optimum thicknesses of each HTL to achieve maximum PCE, the visual comparison is used. Table 3 presents a comparative analysis of power conversion efficiencies (PCEs) for $CH_3NH_3SnI_3$-based PSCs utilizing various HTLs. The initial four entries highlights the efficiencies achieved in this study with different HTLs. $TCO/C_{60}/CH_3NH_3SnI_3$/TAPC configuration as attaining the highest optimised PCE of 31.82%. The subsequent four entries summarize maximum efficiencies reported in other studies for similar tin-based PCEs, showcasing performance

 © Ariston Publications 2026. All rights reserved.

variations across different device architectures and materials.

4. CONCLUSION

The TCO/C_{60}/$CH_3NH_3SnI_3$/TAPC configuration achieves an optimized PCE of 31.82%, with TAPC demonstrating over 90% quantum efficiency across the 400–900 nm wavelength range. Tin-based perovskites like $CH_3NH_3SnI_3$ offer a non-toxic alternative to lead-based counterparts, combining high performance, stability, and cost-effectiveness. In perovskite solar cells, TAPC functions as an efficient HTL, improving stability and efficiency due to its hydrophobic nature, which guards against moisture-induced degradation, and favourable energy alignment. Future research should focus on refining HTLs like TAPC to further improve efficiency, exploring new HTL materials compatible with $CH_3NH_3SnI_3$, and investigating advanced materials to replace traditional transparent conductive oxides (TCOs) with more cost-effective and efficient alternatives. Ensuring long-term stability alongside high efficiency is crucial for the practical application of PSCs. Apart from the advantages, a severe limitation of Tin based PSC is it's Sn2+oxidation but due to some strategies like Antioxidant additives like cesium trifluoroacetate, 2D material integration and coordination chemistry(use of coordination nanosheets) are the different techniques by which the oxidation issue of Sn based perovskite can be minimized.

DECLARATIONS

Ethical Approval

We affirm that this manuscript is an original work, has not been previously published, and is not currently under consideration for publication in any other journal or conference proceedings. All authors have reviewed and approved the manuscript, and the order of authorship has been mutually agreed upon.

Funding

There are no funding

Availability of data and material

All of the data obtained or analyzed during this study is included in the report that was submitted.

Conflicts of Interest

The authors declare that they have no financial or personal interests that could have influenced the research and findings presented in this paper. The authors alone are responsible for the content and writing of this article.

Author's Contributions

A. U.: Conceptualization (equal), Writing - review and editing (equal), Supervision (lead), **N.M.:** Writing - review and editing (equal), **D.K.D:** Supervision, review (equal). All authors have read and agreed to the published version of the manuscript.

Acknowledgments

The authors are extending their sincere thanks to Professor Marc Burgelman and his team at the University of Ghent, Belgium for developing SCAPS-1D simulation software. This powerful and widely known simulation tool has allowed the authors to extensively analyze and optimize solar cell structures throughout this research. The software's user-friendly interface and great functionality allowed the authors to obtain depth in quality of research.

REFERENCES

[1] Couderc, E., **2017**. Perovskite Photovoltaics: Manufacturing Costs. *Nature Energy*, 2, p.17080. https://doi.org/10.1038/nenergy.2017.80.

[2] Umar, Ahmad , Sadan, , Singh, Pravin Kumar , Dwivedi, D. K. , Algadi, Hassan , Alhammai, Mohsen A. M. , Baskoutas, Sotirios, **2022**. High Power-Conversion Efficiency of Lead-Free Perovskite Solar Cells: A Theoretical Investigation. *Micromachines*, 13(12), p.2201. https://doi.org/10.3390/mi13122201.

[3] Sharma, D. , Mehra, R. , Raj, B., **2020**. Materials , Methods for Performance Enhancement of Perovskite Photovoltaic Solar Cells: A Review. *Recent Advances in Power Systems*, 699, p.531-542. https://doi.org/10.1007/978-981-15-7994-3$_4$9.

[4] Yue, L. , Yan, B. , Attridge, M. , Wang, Z., **2016**. Light Absorption in Perovskite Solar Cell: Fundamentals , Plasmonic Enhancement of Infrared B, Absorption. *Solar Energy*, 124, p.143-152. https://doi.org/10.1016/j.solener.2015.11.028.

© Ariston Publications 2026. All rights reserved.

[5] Sadan, Dwivedi, D. K., **2019**. Theoretical Investigation on Enhancement of Output Performance of CZTSSe Based Solar Cell. *Solar Energy*. https://doi.org/10.1016/j.solener.2019.09.079.

[6] Sharma, D. , Mehra, R. , Raj, B., **2021**. Comparative Analysis of Photovoltaic Technologies for High Efficiency Solar Cell Design. *Superlattices , Microstructures*, 153. https://doi.org/10.1016/j.spmi.2021.

[7] Singh, Y. K. , Dwivedi, D. K. , Lohia, Pooja , P,ey, Rahul, **2025**. Current Matching , Filtered Spectrum Analysis of Wide-B,gap/Narrow-B,gap Perovskite/CIGS T,em Solar Cells: A Numerical Study of 34.52% Efficiency Potential. *Journal of Physics , Chemistry of Solids*, 196, p.112300. https://doi.org/10.1016/j.jpcs.2024.112300.

[8] Nahiduzzaman, Md Nahiduzzaman , Shah, Md Salman , Mamur, Hayati , Hasen, Rakib, **2024**. Optimizing Lead-Free CH3NH3SnI3 Perovskite Solar Cells by Using SCAPS-1D Software. *Chemistry of Inorganic Materials*, 4.

[9] Sharma, D. , Mehra, R. , Raj, B., **2022**. Optimization of Tin Based Perovskite Solar Cell Employing CuSbS2 as HTL: A Numerical Simulation Approach. . https://doi.org/10.1007/s12633-022-01691-x.

[10] Zair, Razika , Ighil, Tala, **2021**. SCAPS Simulation for Perovskite Solar Cell. *Journal of Solar Energy Research*. https://doi.org/10.31875/2410-2199.2021.08.3.

[11] Tripathi, Manas , Vaibhav, Vipul , Sengar, Brajendra S., **2022**. Lead Free Perovskite Solar Cell by Using SCAPS-1D: Design , Simulation. *Materials Today: Proceedings*. https://doi.org/10.1016/j.matpr.2022.04.832.

[12] Kumar, Ajay , Punetha, Deepak , Chakrabarti, Subhan,a, **2023**. Performance Optimization of Phenylethylammonium-Formamidinium Tin Iodide Perovskite Solar Cell by Contrasting Various ETL , HTL Materials. *Journal of Nanoparticle Research*. https://doi.org/10.1007/s11051-023-05702-9.

[13] Ahamed, Tanzir , Imteazrahaman , Karmakar, Subrata , Halim, Md Abdul , Sarkar, Pallab Kumar, **2022**. Thickness Optimization , Effect of Different Hole Transport Materials on Methylammonium Tin Iodide (CH3NH3SnI3)-Based Perovskite Solar Cell. *Journal of Emergent Materials*. https://doi.org/10.1007/s42247-022-00405-8.

[14] Mohanty, Ipsita , Singh, Udai P. , Mangal, Sutanu, **2025**. Optical Characterization , Performance Analysis of Tin-Based Perovskite Solar Cells: Experimental , Theoretical Study. *Materials Today Communications*, p.112297. https://doi.org/10.1016/j.mtcomm.2025.112297.

[15] Verma, A. A. , Dwivedi, D. K. , Lohia, Pooja , P,ey, Rahul , Madan, J. , Agarwal, S. , Kulshrestha, U., **2025**. Innovative Design Strategies for Solar Cells: Theoretical Examination of Linearly Graded Perovskite Solar Cell with PTAA as HTL. *Journal of Physics , Chemistry of Solids*, 196, p.112401. https://doi.org/10.1016/j.jpcs.2024.112401.

[16] Bhardwaj, Km Shivani , Rai, Shambhavi , Sadan, , Lohia, Pooja , Dwivedi, D. K., **2021**. Investigating the Performance of Mixed Cation Mixed Halide-Based Perovskite Solar Cells Using Various Hole-Transport Materials by Numerical Simulation. *Optical , Quantum Electronics*, 53, p.602. https://doi.org/10.1007/s11082-021-03262-7.

[17] Burschka, J. , Pellet, N. , Moo, S.-J. , Baker, R.-H. , Gao, P. , Nazeeruddin, M. K. , Gratzel, M., **2013**. Sequential Deposition as a Route to High-Performance Perovskite-Sensitized Solar Cells. *Nature*, 499, p.316-319. https://doi.org/10.1038/nature12340.

[18] Yoon, H. , Kang, S. M. , Lee, J.-K. , Choi, M., **2016**. Hysteresis-Free Low-Temperature-Processed Planar Perovskite Solar Cells with 19.1% Efficiency. *Energy & Environmental Science*, 7(9), p.2262-2266. https://doi.org/10.1039/C6EE01037G.

[19] Saliba, M. , Matsui, T. , Seo, J.-Y. , Domanski, K. , Baena, J.-P. C. , Nazeeruddin, M. K. , Zakeeruddin, S. M. , Tress, W. , Abate, A. , Hagfeldt, A. , Gratzel, M., **2016**. Cesium-Containing Triple Cation Perovskite Solar Cells: Improved Stability, Reproducibility , High Efficiency. *Energy & Environmental Science*, 9(6), p.1989-1997. https://doi.org/10.1039/C5EE03874J.

[20] Shao, Y. , Xiao, Z. , Bi, C. , Yuan, Y. , Huang, Y., **2014**. Origin , Elimination of Photocurrent Hysteresis by Fullerene Passivation in CH3NH3PbI3 Planar Heterojunction Solar Cells. *Nature Communications*, 5, p.5784. https://doi.org/10.1038/ncomms6784.

 © Ariston Publications 2026. All rights reserved.

[21] Ou, Y. , Lu, Z. , Lu, J. , Zhong, X. , Chen, P. , Zhou, L. , Chen, T., **2022**. Boosting the Stability , Efficiency of Cs2AgBiBr6 Perovskite Solar Cells via Zn Doping. *Optical Materials*, 129, p.112452. https://doi.org/10.1016/j.optmat.2022.112452.

[22] Chauhan, Pratibha , Agarwal, Surbhi , Srivastava, Vaibhav , Maurya, Sadan, , Lohia, Pooja , Dwivedi, D. K., . Impact on Generation , Recombination Rate in Cu2ZnSnS4 (CZTS) Solar Cell for Ag2S , In2Se3 Buffer Layers with CuSbS2 Back Surface Field Layer. *Progress in Photovoltaics: Research , Applications*. https://doi.org/10.1002/pip.3743.

[23] Taheri, S. , Kordbacheh, A. A. , Minbashi, M. , Hajjiah, A., **2021**. Effect of Defects on High Efficient Perovskite Solar Cells. *Optical Materials*, 111, p.110601. https://doi.org/10.1016/j.optmat.2020.110601.

[24] Verma, Akash An, , Dwivedi, D. K., **2025**. Boosting Lead-Free Solar Efficiency: Gradient B, Alignment Coupled with ETL Engineering in Chalcogenide Perovskite Solar Cells. *International Journal of Modern Physics B*. https://doi.org/10.1142/S0217979225502522.

[25] Verma, Akash An, , Dwivedi, D. K., **2025**. Advancing RbGeBr3 Perovskite Solar Cells with Metal-Doped Chalcogenide ETL: A Leap Towards Higher Efficiency. *Electrochimica Acta*. https://doi.org/10.1016/j.electra.2025.146950.

[26] Verma, Akash An, , Dwivedi, D. K., **2025**. Performance Benchmarking of Lead-Free Double Perovskites: Design Optimization , Comparative Analysis of Inorganic Cs2BX6 (B = Sn, Pd, X = Br, I) Perovskites for Efficient PSCs. *Journal of Inorganic , Organometallic Polymers , Materials*. https://doi.org/10.1007/s10904-025-03983-2.

[27] Zhang, J. , Wang, L. , Jiang, C. , Cheng, B. , Chen, T. , Yu, J., **2021**. CsPbBr3 Nanocrystal Induced Bilateral Interface Modification for Efficient Planar Perovskite Solar Cells. *Advanced Science*, 8, p.2102648. https://doi.org/10.1002/advs.202102648.

[28] Jeong, J. , Kim, M. , Seo, J. , Lu, H. , Ahlawat, P. , Mishra, A. , Yang, Y. , Hope, M. A. , Eickemeyer, F. T. , Kim, M. , Yoon, Y. J. , Choi, I. W. , Darwich, B. P. , Choi, S. J. , Jo, Y. , Lee, J. H. , Walker, B. , Zakeeruddin, S. M. , Emsley, L. , Rothlisberger, U. , Hagfeldt, A. , Kim, D. S. , Gratzel, M. , Kim, J. Y., **2021**. Pseudo-Halide Anion Engineering for Alpha-FAPbI3 Perovskite Solar Cells. *Nature*, 592(7854), p.381-385. https://doi.org/10.1038/s41586-021-03406-5.

[29] Li, S. , Cao, Y.-L. , Li, W.-H. , Bo, Z.-S., **2021**. A Brief Review of Hole Transporting Materials Commonly Used in Perovskite Solar Cells. *Rare Metals*, 40(10), p.2712-2729. https://doi.org/10.1007/s12598-020-01691-z.

[30] Roy, P. , Sinha, N. K. , Khare, A., **2021**. An Investigation on the Impact of Temperature Variation over the Performance of Tin-Based Perovskite Solar Cell: A Numerical Simulation Approach. *Materials Today: Proceedings*, 39, p.2022-2026. https://doi.org/10.1016/j.matpr.2020.09.281.

[31] Rai, N. , Ravi, S. , Singh, P. K. , Lohia, P. , Dwivedi, D. K., **2020**. Analysis of Various ETL Materials for an Efficient Perovskite Solar Cell by Numerical Simulation. *Journal of Materials Science: Materials in Electronics*, 31, p.16269-16280. https://doi.org/10.1007/s10854-020-04175-z.

[32] Liu, X. , Liu, Z. , Ye, H. , Tu, Y. , Sun, B. , Tan, X. , Shi, T. , Tang, Z. , Liao, G., **2018**. Novel Efficient C60-Based Inverted Perovskite Solar Cells with Negligible Hysteresis. *Electrochimica Acta*, 288, p.115-125. https://doi.org/10.1016/j.electacta.2018.09.004.

[33] Golubev, T. , Liu, D. , Lunt, R. , Duxbury, P., **2019**. Underst,ing the Impact of C60 at the Interface of Perovskite Solar Cells via Drift-Diffusion Modelling. *AIP Advances*, 9, p.035026. https://doi.org/10.1063/1.5068690.

[34] Sherkar, T. S. , Momblona, C. , Escrig, L. G. , Avila, J. , Sessolo, M. , Bolink, H. J. , Koster, L. J. A., **2017**. Recombination in Perovskite Solar Cells: Significance of Grain Boundaries, Interface Traps, , Defect Ions. *ACS Energy Letters*, 2(5), p.1214-1222. https://doi.org/10.1021/acsenergylett.7b00236.

© Ariston Publications 2026. All rights reserved.